DOI: 10.1002/ejic.200800910

Mixed Valency at the Nearly Delocalized Limit: Fundamentals and Forecast

Starla D. Glover,[a] John C. Goeltz,[a] Benjamin J. Lear,[a] and Clifford P. Kubiak*[a]

Keywords: Mixed-valent compounds / Electron transfer / Spectroelectrochemistry / Self-assembly / Ruthenium

Mixed valency is important in many areas of chemistry, from synthetic to biological systems, from the simplest systems to the most highly complex. The purpose of our research is to understand the principles of mixed valency in localized, nearly delocalized, and delocalized systems, and to apply our knowledge to the rational design of molecular devices. This microreview discusses our group's research over the last ten years. It reviews methods of estimating picosecond electron-transfer lifetimes from infrared spectral lineshapes, studies of the localized-to-delocalized transition and the effects of frozen solvents, charge gating by non-covalent interactions, electron-transfer-gated electron transfer, and the distribution of charge within a molecule probed and controlled by an applied electric field.

1. Introduction

The year 2007 marked the fortieth anniversary of the seminal findings of Robin, Day, Creutz, Taube, and Hush on the classification, synthesis, and physical properties of inorganic mixed-valence ions.[1,2] For all that we have learned in the past forty years about inorganic mixed valency, there is still much that we do not know. In this microreview we take a look at the current frontiers of inorganic mixed-valence chemistry, and attempt to point out directions where important future discoveries may be made.

In 1997, we began the study of a class of mixed-valence complexes composed of dimers of ruthenium trimers, Figure 1. These compounds share a number of characteristics which make them amenable to a wide variety of studies, from those purely physical in nature to those which lay the groundwork for future device applications. Our early investigations were focused on the effects of picosecond intramolecular electron transfer in the mixed-valence state on vibrational spectra.[3] Variability of ligands in the ancillary positions ("L" in Figure 1) enabled us to synthesize mixed-valence species from moderately electronically coupled (exchanging electron localized) to highly electronically coupled (exchanging electron delocalized).[4] The CO ligand has proven to be a valuable spectroscopic "reporter" of the redox state and exchange rate between inequivalent sites. IR spectra of ν(CO) stretching modes show clear evidence of dynamic coalescence, an indication that exchange occurs on, or near, the vibrational timescale.[3] These spectroscopic characteristics allow for a detailed investigation of the localized to delocalized transition and picosecond dynamics in solution.[5]

[a] Chemistry and Biochemistry, University of California, San Diego,
9500 Gilman Drive, 92093-0955 La Jolla, California, USA
Fax: +1-858-534-5383
E-mail: ckubiak@ucsd.edu

Starla Glover (left) was born in Lewiston, Idaho in 1979. In 2005 she received her BS with honors in chemistry from Portland State University in Portland, Oregon. Since 2005, Starla has been pursuing a PhD under the supervision of Professor Kubiak at University of California, San Diego. From her studies, Starla hopes to gain a more complete physical understanding of the Class II/III borderline in mixed-valence complexes. In addition to chemistry, Starla also enjoys cycling, knitting, and dark chocolate.

John Goeltz (second from right) received his BS in chemistry from Yale University in 2003. After briefly pretending to be a rock star, he began his PhD studies at UC San Diego on mixed-valence self assembled monolayers. John enjoys strong ales and turntables.

Benjamin Lear (right) received his BS from University of California, Davis, and his PhD with Prof. Kubiak in 2007. He is currently doing post-doctoral research with Prof. Malcolm Chisholm at The Ohio State University. In between time spent doing research, reading, and cooking, he plays Frisbee.

Clifford Kubiak (second from left) is the Harold C. Urey Distinguished Professor of Chemistry at the University of California, San Diego. Kubiak received the Sc. B. degree with honors in chemistry from Brown University in 1975. He was awarded the Ph. D. (1980) in chemistry by the University of Rochester, and then pursued postdoctoral studies in photoelectrochemistry in 1980–1981 with Mark S. Wrighton at M. I. T. Kubiak's research is in inorganic electron transfer, carbon dioxide utilization, and molecular electronics.

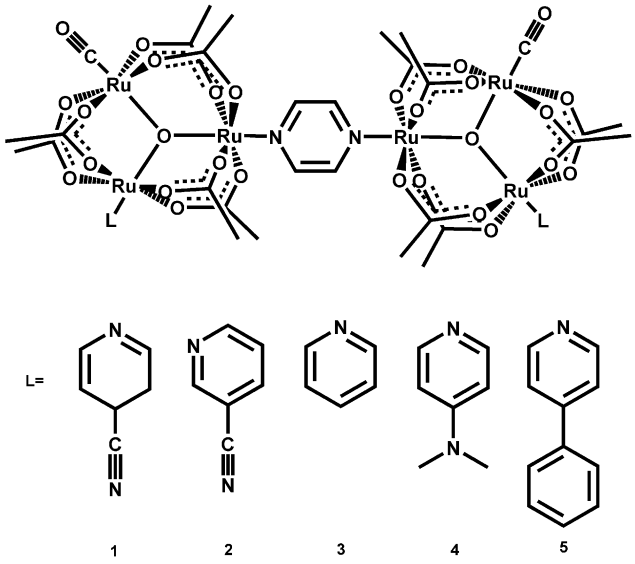

Figure 1. Dimers of pyrazine (pz)-bridged ruthenium trimers. In neutral complexes the formal oxidation states of ruthenium metal centers are $Ru_3^{III,III,II}$–pz–$Ru_3^{III,III,II}$. In the mixed-valence state the complexes are monoanions and oxidation states on the ruthenium atoms are $Ru_3^{III,II,II}$–pz–$Ru_3^{III,III,II}$.

Our improved understanding of these areas at the forefront of physical inorganic chemistry led us to explore ways to design and control charge distribution in solution and in self-assembled monolayers (SAMs). The following sections describe our recent studies that began with some of the first reported rate constants for picosecond ground-state electron transfer in mixed-valence ions and progressed to controlled gating of electron transfer in solution and probing the polarizability of monolayers of mixed-valence compounds with an electric field.

2. Solvent Effects in Nearly Delocalized Complexes

In recent years many inorganic chemists have been concerned with attaining a clear understanding of the Class II/III borderline for mixed-valence complexes. This is, after all, the most fundamental question in mixed-valence chemistry: is the system localized or delocalized? Mixed-valence complexes have been classified by their electronic, solvent, and vibrational motions.[1] In Class II complexes the exchanging electron and solvent are taken to be localized. In Class III complexes the electron is delocalized and the surrounding solvent is averaged. In his 2001 review, Meyer attempted to provide a concise definition of "borderline" Class II/III behaviour: in Class II/III complexes the exchanging electron is localized and the solvent is averaged.[6] Many attempts have been made to define the localized to delocalized transition by quantitative analysis of intervalence charge-transfer (IVCT) bands. In our work, we have been able to directly address the localized to delocalized transition of our nearly delocalized mixed-valence systems by IR spectral analysis of the effect of solvent dynamics upon the rates of electron transfer.[7,8] The key concept is that if a mixed-valence species rests at the Class II/III borderline, it must be nearly delocalized, and the barrier for intramolecular electron transfer should be nearly zero. In this regime, *pre-exponential* terms in the normal rate expression for ET will come into play. The ET rate expression for a symmetric mixed-valence complex with no driving force is given by [Equation (1)][9]

$$k_{ET} = \kappa\, \nu_N \exp[-(\Delta G_\lambda^* - H_{AB} + H_{AB}^2/4\ \Delta G_\lambda^*)/RT] \quad (1)$$

and depends on the transition probability, κ ($\kappa = 1$ for adiabatic systems), the nuclear frequency factor, ν_N, electronic coupling, H_{AB}, and the thermal activation barrier, ΔG_λ^* [where $\Delta G_\lambda^* = (\lambda - 2H_{AB})^2/4\lambda$ and λ is the vertical reorganization energy]. In Class II/III systems, H_{AB} approaches $\lambda/2$ and the rate of electron transfer begins to depend on the frequency factor, ν_N, in the preexponential term, which is a weighted average of the inner-sphere and outer-sphere motional modes that contribute to the electron-transfer reorganization energy. For intramolecular ET reactions in solution, these modes include solvent frequencies and intramolecular vibrations that promote ET. Because the timescale for solvent dynamics is very fast, the effects of solvent dynamics are usually seen only in very fast electron transfers, such as those proceeding from electronic excited states.[10]

Figure 2 shows the solvent dependence of ν(CO) spectra in the IR for dimer $\mathbf{3}^-$ in acetonitrile, dichloromethane, and tetrahydrofuran with estimated electron-transfer rate constants in the terahertz regime. Rate constants for electron transfer are obtained from simulations based on modified Bloch equations analogous to those used in dynamic NMR coalescence. The theory behind these simulations is detailed in a review written by Turner.[11] We have carefully considered the effect of solvent on electron-transfer rates, where a host of solvent thermodynamic (time-independent) parameters and dynamic (time-dependent) parameters were com-

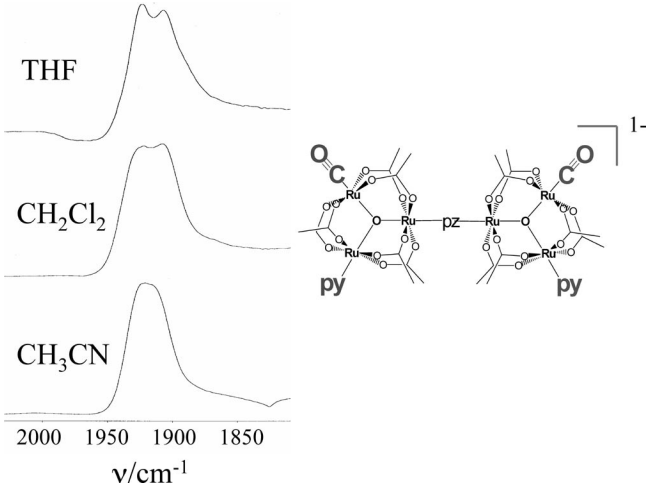

Figure 2. IR bandshapes for the ν(CO) stretch of $\mathbf{3}^-$ in CH_3CN, CH_2Cl_2 and THF where estimated electron-transfer rate constants are $2.6 \times 10^{12}\ s^{-1}$, $1.8 \times 10^{12}\ s^{-1}$, and $1.1 \times 10^{12}\ s^{-1}$, respectively. More coalesced spectra are associated with faster rates of electron transfer.

pared.[8] We concluded that in the nearly delocalized limit, solvent thermodynamic parameters do not significantly impact rates of electron transfer. The time-independent parameters we examined were the solvent reorganization energy, optical and static dielectric constants, and solvent polarity. Commonly, rates of ET depend on the solvent reorganization energy, as seen in Class II systems. This is not the case for our systems, as can be seen from the plot (a) in Figure 3 where the ET lifetimes of four symmetric mixed-valence dimers in seven different solvents are plotted vs. the solvent reorganization energies. The extremely poor linear correlation points to a profound absence of solvent reorganizational influence on k_{ET}. This result shows that as the barrier to ET approaches zero, the solvent reorganizational contribution to the barrier becomes unimportant.

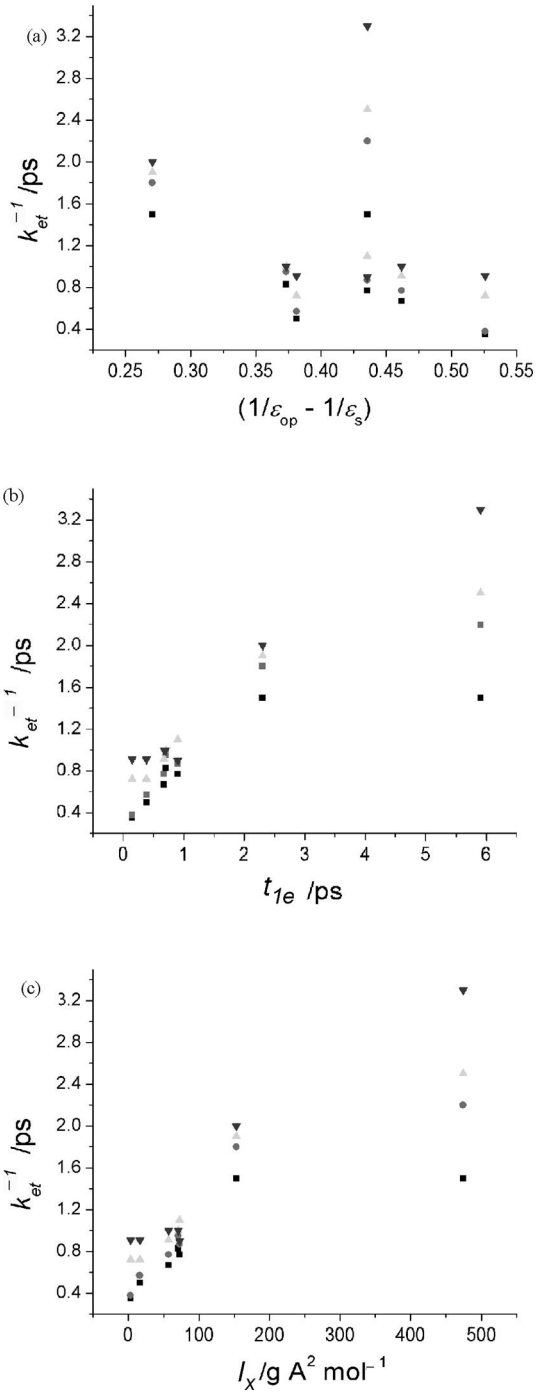

Figure 3. Electron-transfer lifetimes of four symmetric dimers, **1**$^-$ (gray inverted triangle), **2**$^-$ (gray triangle), **3**$^-$ (gray circle), and **4**$^-$ (black square), are plotted vs. various solvent parameters. The solvents used in this study are CH_3CN, CH_2Cl_2, DMF, THF, DMSO, $CHCl_3$, and HMPA. a) Plot of ET lifetime vs. $(1/\varepsilon_{op} - 1/\varepsilon_s)$, the variable portion of the outer-sphere reorganization energy, λ_o. b) Plot of ET lifetime vs. the characteristic solvent relaxation time, t_{1e}. **c**) Plot of ET lifetime vs. the moment of inertia along the solvent's *x*-axis.

This becomes clearer upon examining time-dependent solvent parameters. The best correlation to electron-exchange lifetime (k_{ET}^{-1}) was with the solvent dipolar reorientation times determined by Maroncelli and co-workers. This group measured the time-resolved Stokes shift in the fluorescence of Coumarin 135 in 24 common organic solvents.[12] In general, these studies show a biexponential solvent response, where the fastest solvent response times are due to solvent inertial (rotational) motion. In part b of Figure 3, the ET lifetime is plotted against the parameter t_{1e}, which encompasses the total evolution of solvent-dynamic response to changes in local environment. For comparison, the lifetimes are also plotted vs. solvent moments of inertia in Figure 3 (c). These plots are almost identical, underscoring the important role of solvent inertial motions in solvent reorientation. This study illustrates that solvent *dynamics* significantly influence ET in the ground state of nearly delocalized mixed-valence complexes.

Of the modes that contribute to ν_N, the solvent dynamics are expected to be the major contributor in fluid solution, as they are slower than internal molecular vibrations. We know from previous resonance Raman studies that electron transfer is mediated in part by the ν_{8a} symmetric stretching frequency of the pyrazine bridging ligand.[13] The frequency of this vibration is 4.8×10^{13} s^{-1}, while the fastest solvent dipolar reorientation frequency of the solvents studied by Maroncelli is 6.7×10^{12} s^{-1} (for acetonitrile).[13] It is clear that solvent relaxation can limit the rate of ET in a Class II/III system. At this point it is interesting to consider what would happen if solvent dynamic modes were decoupled from electron transfer. Would the observed rate of electron transfer increase or decrease?

3. Non-Arrhenius Behaviour in Frozen Solvents

Decoupling fast solvent reorientations from ET was achieved by freezing solutions of a mixed-valent dimer.[14] One expected consequence is that the dynamic solvent reorientation will no longer contribute to the pre-exponential term and ν_N will include a more heavily weighted average of inner sphere (molecular) vibrations. Parts a and b of Figure 4 show ν(CO) stretches of **1**$^-$ in acetonitrile and dichloromethane at decreasing temperatures.[8] These spectra show that as the solution approaches its freezing point, the degree of ν(CO) spectral coalescence increases. Once the solvent is frozen (–92 °C for dichloromethane and –44 °C

for acetonitrile), completely coalesced bandshapes are observed. Cooling the solvent beyond its freezing point brings about no further changes in the ν(CO) bandshape. Lifetimes for ET were obtained by spectral simulation and are given for each temperature.[15] The key conclusion regarding Figure 4 is that as the solvent is cooled to its freezing point, k_{ET} increases, and once the solvent is frozen k_{ET} remains the same. These results demonstrate a localized to delocalized transition at the freezing point, where solvent dynamics become largely uncoupled from electron transfer and internal vibrational modes of the molecule dominate ν_N.

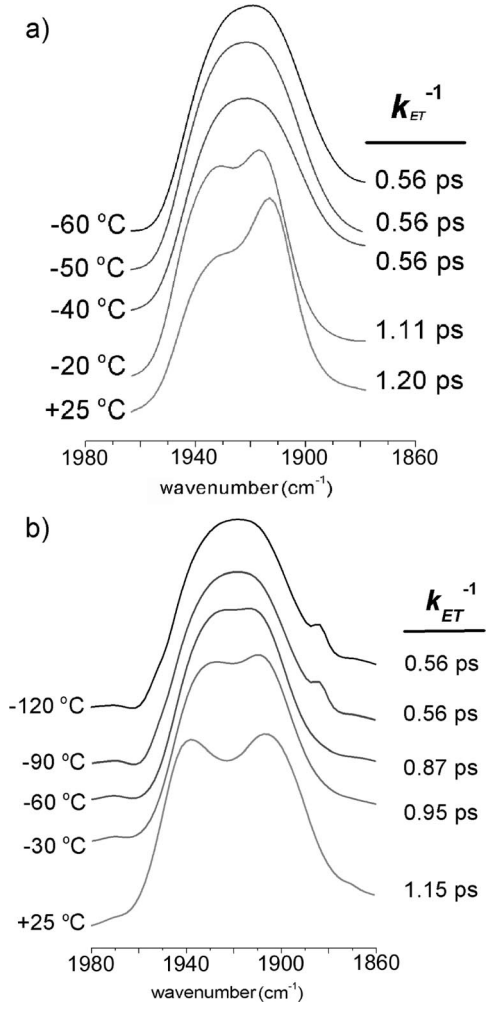

Figure 4. IR band shapes for ν(CO) of the mixed-valence dimer, **1**$^-$, in acetonitrile (top) and dichloromethane (bottom) as a function of temperature. The mixed-valence anion was produced by a chemical reduction with 1.1 molar equivalents of cobaltocene. The band shape shows increasing coalescence as temperature is reduced. Electron-transfer lifetimes obtained from spectral simulation are listed to the right of each spectrum.

The studies described above allow for a more complete picture of mixed valency at the Class II/III borderline. Rates of intramolecular electron transfer in nearly delocalized systems are highly dependent on solvent *dynamics* and not solvent thermodynamic parameters. Clearly, the solvent does not appear averaged to the exchanging electron, but limits in a motional sense how fast the electron can exchange. Decoupling solvent modes from ET reveals this fact unambiguously. A precise definition of Class II/III mixed-valence compounds that follows from our research is that solvent-dynamical parameters control the rates of ET in borderline complexes, and tend to localize otherwise delocalized electronic states.

4. Restoration of Broken Symmetry as a Driving Force for Cooperative Noncovalent Host–Guest Chemistry

Current research within the fields of supramolecular chemistry and molecular electronics hinges on the need to understand the directed self assembly of functional nanostructures.[16] It is commonly understood that cooperative interactions between molecules are a necessity in "guided" self assembly processes. Also, it is highly desirable to develop functional molecular devices that operate in the terahertz regime. Here, we describe studies in which our mixed-valence complexes act as the guest molecule in a cooperative non-covalent binding event with calix[6]arene, a host molecule. The symmetry of the mixed-valence ion **5**$^-$ (Figure 1) is broken by the binding of a single calix[6]arene and is accompanied by a decrease in the stabilization of the mixed-valence state. The energetic gain provided by the restoration of symmetry drives binding of a second calix[6]arene in a cooperative fashion.[17]

It is well known that calix[6]arene plays host to aromatic compounds.[18] In our system this is realized by the reversible binding of calix[6]arene to the phenyl group on the ancillary 4-phenylpyridine ligand. This interaction leads to behaviour which is similar to that of "mixed-valence isomers,"[19] with the important difference that the asymmetry in this system is not a permanent manifestation of the connectivity of molecules, but rather is present in the following dynamic equilibrium [Equation (2)].

5$^-$ + 2 [calix[6]arene] ↔ [**5**$^-$][calix[6]arene] + [calix[6]arene] ↔ [**5**$^-$][calix[6]arene]$_2$ (2)

Cyclic voltammetry (CV) and differential pulse voltammetry (DPV) experiments were used to deduce the energetics of this type of supramolecular system. The CV of **5** in dichloromethane shows two reversible one-electron reductions with half-wave potentials ($E_{1/2}$) of –1.126 V and –1.500 V vs. Fc/Fc$^+$ corresponding to an electron being added to each cluster sequentially. The electrochemical splitting in a symmetric mixed-valence system, $\Delta E_{1/2}$, is a qualitative measure for the amount of electronic coupling that exists between electron donor and acceptor.[20] $\Delta E_{1/2}$ for this process is 374 mV, and indicates a high degree of electronic coupling.

A series of DPV experiments were performed on **5** with successive titrations of calix[6]arene. Figure 5 shows forward and reverse scans in the presence of 0.0 and 6.0 molar equivalents of calix[6]arene. There are three important points to mention about this data which are summarized in Scheme 1. First, the potential of the first reduction, $E_{1/2}$(1),

changes by –2 mV. Second, the potential of the second reduction, $E_{1/2}(2)$, changes by +19 mV. Third, the change in $\Delta E_{1/2}$ (i.e. $\Delta\Delta E_{1/2}$) upon the addition of 6.0 molar equivalents of host is –21 mV.

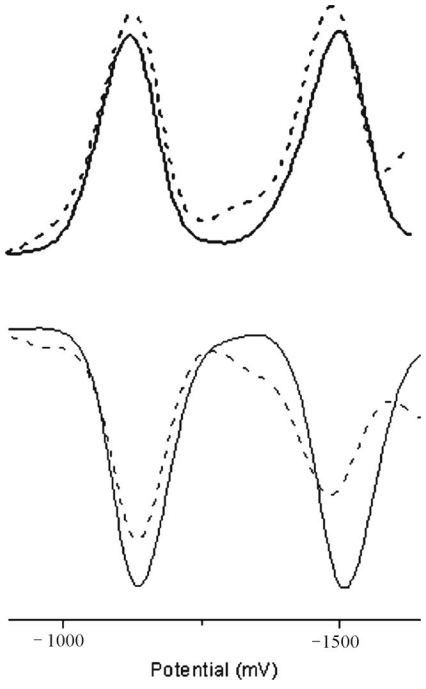

Figure 5. Forward (top) and reverse (bottom) DPV scans of a 2 mM solution of **5** in CH_2Cl_2 with 0.1 M TBAH with 0.0 equiv. of calix[6]arene (solid lines) and 6.0 equiv. of calix[6]arene (dashed lines). Potentials are vs. Fc/Fc^+ couple.

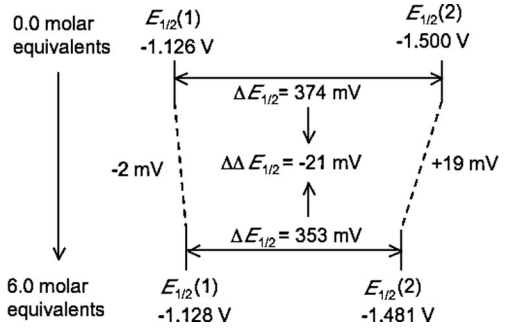

Scheme 1. Halfwave potentials from DPV for the first and second reductions of **5** in the presence of no calix[6]arene (top) and 6.0 molar equivalents of calix[6]arene (bottom). The change in potential of the first reduction, $E_{1/2}(1)$, is –2 mV and the second reduction, $E_{1/2}(2)$, is +19 mV. The total change in electrochemical splitting, $\Delta\Delta E_{1/2}$, is –21 mV.

The overall observed shifts in the reduction waves of **5** can be understood in terms of two different electronic perturbations: inductive and resonance stabilization. We first consider the inductive stabilization. Upon the binding of calix[6]arene to the 4-phenylpyridine ligand, the pK_a of the ligand is decreased. This has the effect of stabilizing the Ru_3 cluster by "inductive effects." Changes in inductive stabilization appear as changes in $E_{1/2}(1)$ and $E_{1/2}(2)$. The change in "resonance stabilization" is reflected in the change in $\Delta E_{1/2}$. $\Delta E_{1/2}$ is related directly to the comproportionation equilibrium constant, K_c, a measure of the thermodynamic stability of a mixed-valence ion arising from electronic delocalization.

The quantitative contributions of the inductive and resonance effects to the observed value of the redox potentials can be separated as follows. The observed change in $\Delta E_{1/2}$ upon binding of calix[6]arene is a decrease by 21 mV. This change should affect $E_{1/2}(1)$ and $E_{1/2}(2)$ symmetrically, i.e. $E_{1/2}(1)$ should shift more negative by 11 mV and $E_{1/2}(2)$ should shift more positive by 11 mV. This implies that the total *observed* shift in $E_{1/2}(1)$ upon addition of 6.0 molar equivalents of calix[6]arene of –2 mV must be the result of a shift of $\Delta\Delta E_{1/2}$ of –11 mV countered by a shift of $E_{1/2}(1)$ by +9 mV. Following the same reasoning, the observed change in $E_{1/2}(2)$ of +19 mV can be resolved as a contribution from $\Delta\Delta E_{1/2}$ of +11 mV, and a contribution from the inductive change in $E_{1/2}(2)$ of +8 mV. The potential shifts in $E_{1/2}(1)$ and $E_{1/2}(2)$ indicate that the binding of calixarene has a slight inductive stabilizing effect of the cluster to which it binds. In contrast, the decrease in $\Delta E_{1/2}$ indicates that calixarene binding slightly decreases the stability of the mixed-valence state by decreasing delocalization.

Plotting $\Delta E_{1/2}$ vs. increasing concentrations of host molecule reveals an additional interesting feature of the binding of calix[6]arene to the mixed-valence ion $\mathbf{5}^-$, Figure 6. The sigmoidal shape of the plot is a clear indication of cooperative binding. That is, the binding of one calix[6]arene to the dimer positively influences the binding of a second calix[6]arene. The observed positive cooperativity of the binding of calix[6]arene to the mixed-valence ion $\mathbf{5}^-$ is a consequence of the loss and restoration of symmetry caused by the binding of one or two calixarene molecules, respectively. This is most easily seen by considering the potential energy surfaces for symmetric and asymmetric mixed-valence compounds. Scheme 2 describes the energetics of our system from the perspective of the Marcus–Hush two-state model for mixed-valence complexes. In stage A, where no calix[6]arene is bound, the potential energy surface describes a symmetric mixed-valence complex. In stage B, the binding of a single calix[6]arene to one of the clusters slightly stabilizes that cluster (inductive effect), and introduces a slight asymmetry to the potential energy curve for $\mathbf{5}^-$. In the singly bound host–guest complex, the energetic offset between the two energy minima is equal to the driving force introduced by calixarene binding, ΔG_0. One important result of 1:1 host–guest binding is that the barrier to electron exchange increases approximately by the amount of driving force present in the asymmetric potential energy surface (ΔG_0). The unavoidable conclusion is that the degree of electron delocalization in the asymmetric 1:1 complex (stage B) is less than in the symmetric case (stage A). The cooperative binding is easily explained by the restoration of symmetry upon binding of the second calix[6]arene. Symmetry restoration eliminates the driving force offset (ΔG_0) from the electron-exchange barrier, and the symmetric 1:2 complex is resonantly stabilized, relative to the asymmetric 1:1 complex.

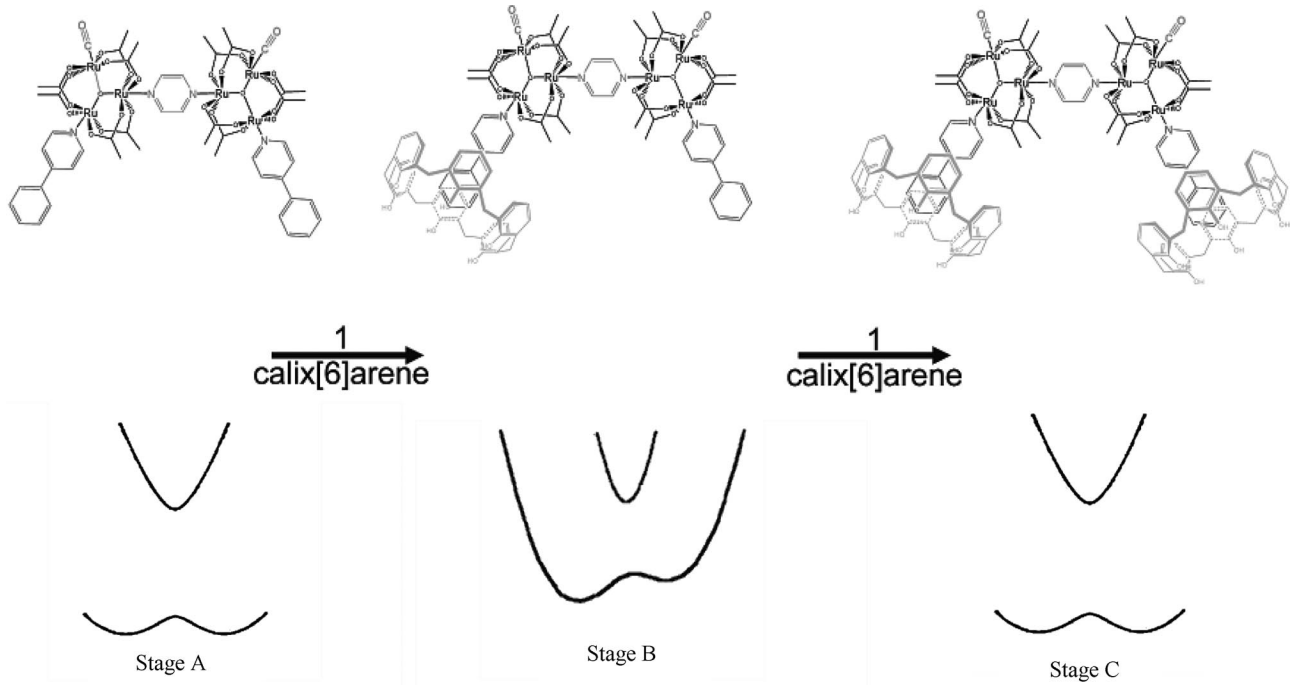

Scheme 2. Stage A – The dimer is in its symmetric uncomplexed form. Stage B – One calix[6]arene binds to the dimer through the 4-phenylpyridine ligand, which provides energetic stabilization to this cluster. This also introduces asymmetry to the dimer as a whole, which decreases the resonance stabilization of the mixed-valence anion. Stage C – Symmetry is restored to the dimer upon the binding of a second calix[6]arene. The binding of the second calix[6]arene is driven by the stabilization to the individual cluster to which it binds, as well as the overall resonance stabilization of the complex. It is this additional resonance stabilization which drives cooperative binding in this system.

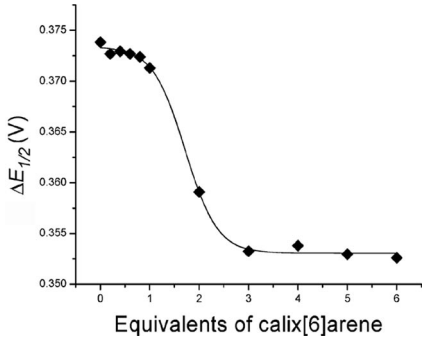

Figure 6. Plot of $\Delta E_{1/2}$ vs. equivalents of calix[6]arene. The sigmoidal curve is fit with an $R^2 = 0.9985$ and a $\chi^2 = 1.987 \times 10^{-7}$. The strong sigmoidal shape of this curve is a clear indication of positive cooperative binding.

This study is another example of the extreme sensitivity of nearly delocalized compounds to their environment. Even the very weak noncovalent binding interactions at the distal positions give rise to perceptible electronic effects within the complex. This work also underscores the importance of the dynamic environment in the energetic landscape of systems undergoing fast exchange. In addition, it demonstrates rudimentary supramolecular control over picosecond electron exchange.

There have been many reported attempts at gating and otherwise controlling electron transfer on the basis of molecular dynamics,[21] pH,[22] magnetism,[23] ion selectivity,[24] and light.[25] In the next two sections, we review our work on two new mechanisms for controlling electronic distribution in a molecule that go beyond our supramolecular work, and expand our understanding of the contributions of local environments. In section 5, electron transfer from donor to acceptor is gated by electron transfer to and from the bridge. In section 6, an applied field probes the polarizability of a mixed-valence self-assembled monolayer.

5. Electron-Transfer-Gated Electron Transfer

The synthetic modularity of the trinuclear ruthenium clusters allows a depth of study unusual in spectroelectrochemical work. Replacing the bidentate pyrazine bridge with tridentate trispyridyltriazine resulted in the zeroth-generation ligand-centered dendrimer (LCD) (**6**), depicted in Figure 7.[26] In the anodic region of the cyclic voltammetric (CV) analysis, this complex displays two separate, reversible three-electron oxidation waves corresponding to the $Ru^{III}Ru^{III}Ru^{II}/Ru^{III}Ru^{III}Ru^{III}$ (+0.17 V vs. Fc/Fc^+) and $Ru^{III}Ru^{III}Ru^{III}/Ru^{III}Ru^{III}Ru^{IV}$ (+0.95 V) couples occurring for each of the three clusters in a concerted manner indicating no electronic communication. In the cathodic region, the cluster reductions are split into two distinct reversible processes. A one-electron reduction at –1.24 V is assigned to the $Ru^{III}Ru^{III}Ru^{II}/Ru^{III}Ru^{II}Ru^{II}$ reduction of one cluster, and a two-electron reduction at –1.36 V is assigned to the concerted reduction of the other two clusters. The one-electron reduction of the triazine bridge is seen at –1.79 V.

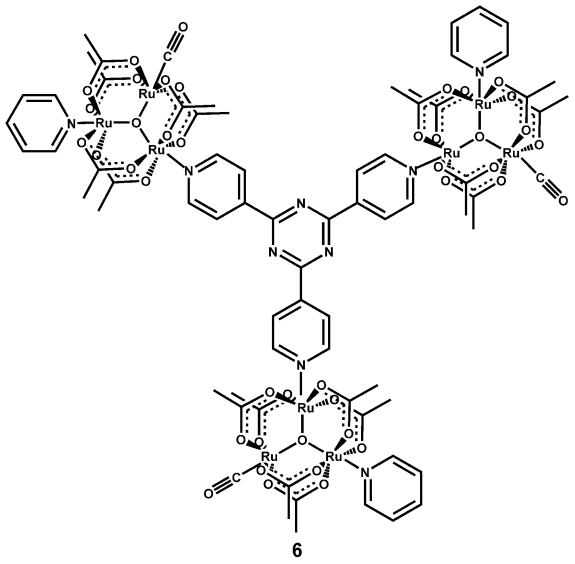

Figure 7. Zeroth-generation ligand-centered dendrimer (LCD) $[Ru_3O(OAc)_6(CO)(py)]_3$-μ_3-2,4,6-tripyridyl-S-triazine.

With these electrochemical assignments and our prior knowledge of the electronic behaviour of the pyrazine-bridged dimers of trimers,[3] the infrared spectroelectrochemical (IR-SEC) response was investigated in order to probe the electronic communication evident in the CV. At low temperature (–30 °C) the ν(CO) region behaves as expected at reducing potentials. As the three clusters are reduced, the ν(CO) of the neutral cluster at 1940 cm^{-1} decreases in intensity, and that of the reduced cluster at 1895 cm^{-1} increases, as shown in Figure 8 (a). At room temperature, the change stops at the point where the intensity ratio indicates two reduced clusters and one neutral cluster (Figure 8, b), and the triazine region (1500–1650 cm^{-1}) indicates that the bridge is reduced (Figure 8, c, d), a feature not seen in the low-temperature spectrum.

In comparing the IR spectra with two reduced clusters and one oxidized cluster at different temperatures (Figure 8, f), dynamic broadening is evident only in the room-temperature experiment. Lineshape analysis equivalent to that discussed earlier yields estimated rate constants for electron transfer of $k_{ET} = 1.1 \times 10^{12}$ s^{-1} at room temperature, and $k_{ET} < 10^{11}$ s^{-1} at low temperature. The relatively small temperature difference is insufficient to explain the observed difference of several orders of magnitude in k_{ET}, and the reduced bridging ligand seen only in the room-temperature spectrum must be invoked. A proposed mechanism explaining the observed phenomena is shown in Scheme 3. Briefly, after three clusters are reduced, one cluster reduces the bridge. This creates an energetically more favourable donor-bridge-acceptor overlap and leads to faster ET. We believe this to be the first reported example of the turn-on of intramolecular electron transfer mediated by an electron-transfer event within the molecule.

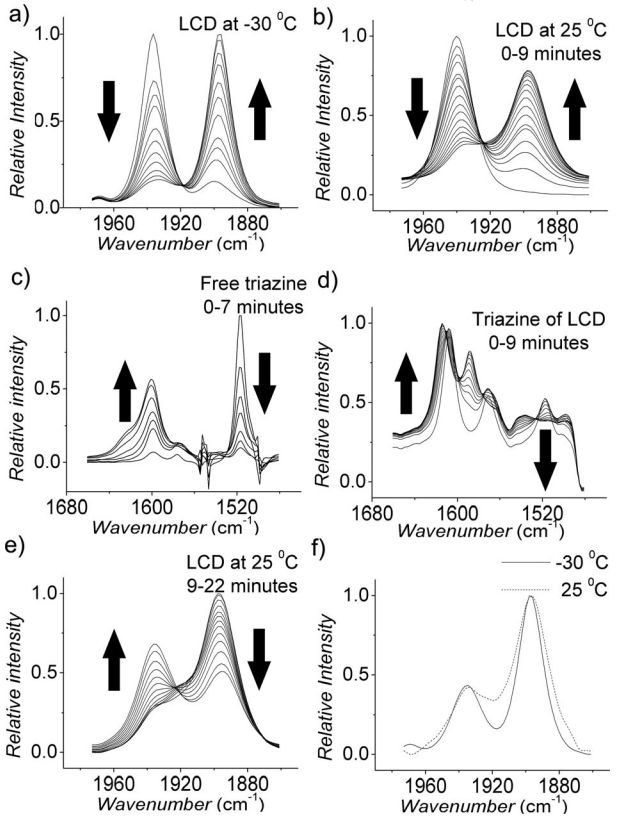

Figure 8. IR spectroelectrochemical response of (a) LCD at –30 °C and –0.95 V, (b) LCD at room temperature and –1.05 V, (c) 2,4,6-tri-4-pyridyl-S-triazine at room temperature and –1.20 V, (d) LCD at room temperature and –1.05 V, (e) LCD at room temperature and –1.05 V after 9 min of electrolysis, and (f) a comparison of the spectra of LCD at –30 °C and room temperature. All potentials are vs. Ag wire.

6. Electric Fields Can Both Control and Probe Oriented Mixed-Valence Compounds

The electron-transfer-gated electron transfer described above led us to extend the idea of charge gating to the application of an electric field. Indeed, relatively little work has been done exploring the electrostatic responses of mixed-valence ions in ordered monolayers,[27] despite the fact that mixed-valence ions fulfil many of the requirements for molecular computing set out by the International Technology Roadmap for Semiconductors, including bistable states and terahertz switching times.[28] In this section we describe our work on effecting changes in charge distribution within a mixed-valence molecule by application of an electric field.[29]

Tetrathiafulvalene (TTF) undergoes two one-electron oxidations, and the monocation TTF^+ has been classified as a delocalized Robin–Day Class III mixed-valence ion.[30] The neutral molecule **7**, shown in Figure 9, was synthesized by the literature procedures[31] and deposited on gold (111) surfaces as a self-assembled monolayer. Electrochemical measurements confirm a surface-bound species and a stable mixed-valence ion. The two reversible oxidations $E_{1/2}(0/+)$

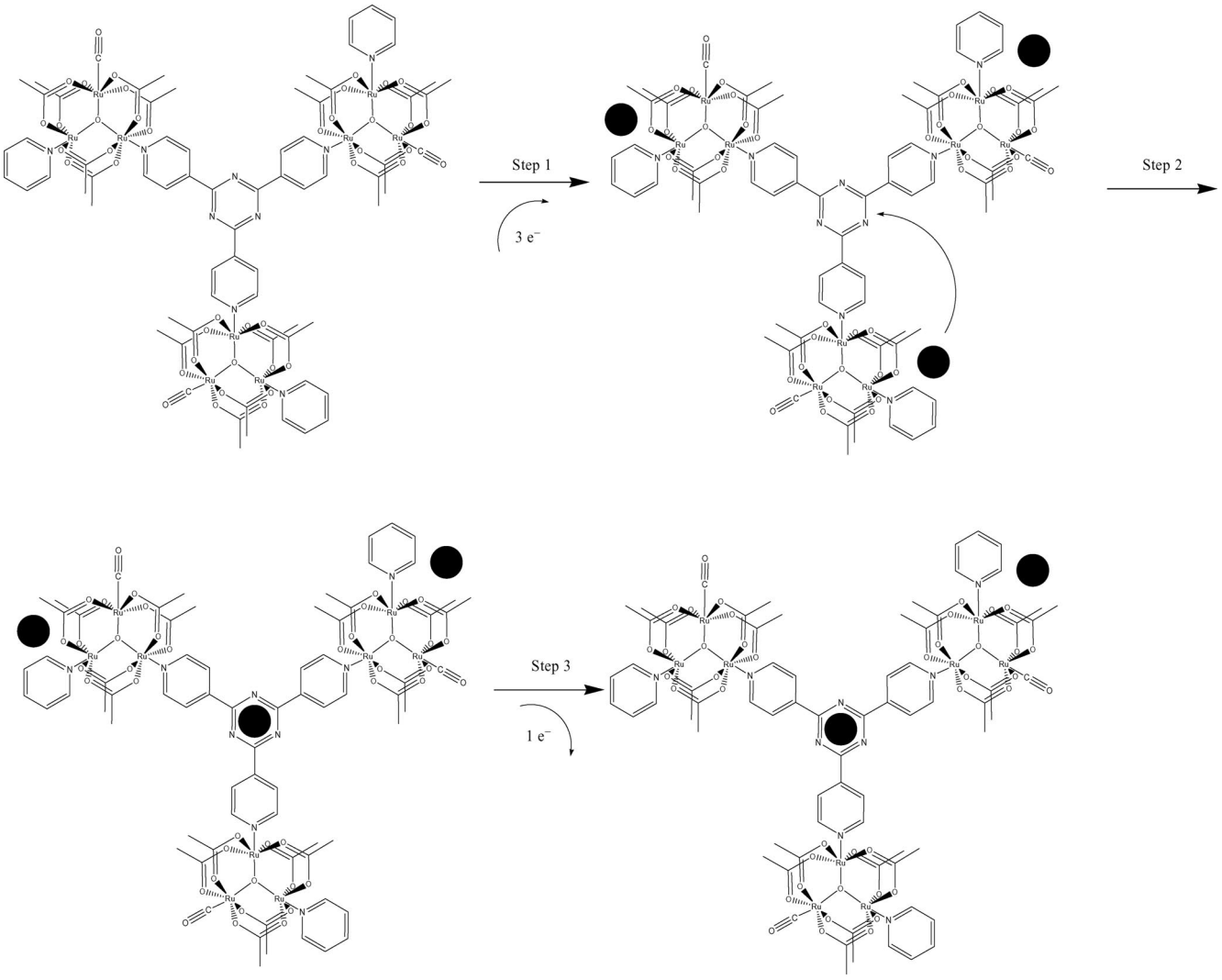

Scheme 3. The LCD initially undergoes a three-electron reduction (step 1). An intramolecular electronic reorganization follows, in which one of the reduced clusters donates an electron to the triazine ligand (step 2). This represents the "turn on" of ultrafast intramolecular ET. Upon its reduction, the triazine pushes the reduction potential of the clusters more negative, resulting in the subsequent oxidation of one of the clusters (step 3).

= –0.00 and $E_{1/2}(+/2^+)$ = +0.40 (vs. Fc/Fc^+ in MeCN) show peak currents proportional to the scan rate and persist without loss on repeated scanning. The narrow bandshapes seen in the surface infrared (PM-IRRAS) analysis qualitatively demonstrate good monolayer ordering.

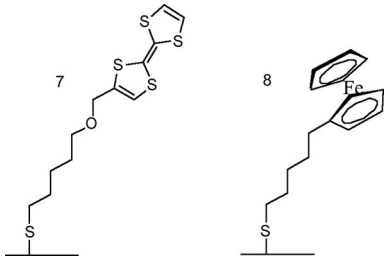

Figure 9. Tetrathiafulvalene (TTF) and ferrocene derivatized for binding to Au: molecules **7** and **8**.

PM-IRRAS was also used to characterize the mixed-valence state $\mathbf{7}^+$. Exposure of neutral SAMs of **7** to ca. 10 mM ferrocenium PF_6^- in CH_2Cl_2 resulted in the appearance of a strong PF_6^- band at 862 cm^{-1}, and new broad bands at ca. 3500, 3200, and 1500 cm^{-1} correspond closely to bands observed in the liquid-phase IR spectrum of TTF^+. A charge-transfer complex SAM of **7** codeposited with tetracyanoethylene (TCNE) was assigned an oxidation state of $\mathbf{7}^{+0.85}$ on the basis of the ν(CN) stretch shifting from 2257 cm^{-1} for free TCNE to 2201 cm^{-1} in the SAM.[32]

Kelvin probe force microscopy (KFM) is often used to determine electric fields (surface potentials or contact-potential differences) due to trapped charges, voltages applied to conducting substrates, or permanent dipoles of the molecular components of SAMs.[33] In the most common KFM experiment, an AC voltage is applied to the tip at its resonant frequency causing an oscillation as the tip be-

comes charged and is alternately attracted and repulsed by a static electric field emanating from the substrate. As a DC voltage between the tip and the substrate is swept, the amplitude of the oscillation changes according to the following proportionality [Equation (3)].

$$A_{\mathrm{RMS}} \propto \frac{\mathrm{d}C}{\mathrm{d}z} V_{DC} V_{AC,RMS} \tag{3}$$

Here, dC/dz is the capacitance (expressed as a gradient because it is dependent on the electrode separation), ΔV_{DC} is the difference between the applied voltage and the negative of the surface potential, and V_{AC} is the AC voltage.[34] The amplitude is minimized when the field from the applied DC voltage nullifies the electric field from the sample, eliminating electrostatic forces felt by the tip. Normally the surface potential is the parameter of interest, but here the *slope of the amplitude response* gives information about the relative capacitances of SAMs of **7**, **7**$^{+}$PF$_6^{-}$, and **7**-TCNE.

The microscope here does not measure the dielectric constant, but simply measures the dipolar field between the gold substrate and the tip as an electric force. The positive charge delocalized on the TTF^{+} group responds to the AC field as depicted in Scheme 4, and the resulting internal dipolar field in the monolayer decreases the capacitance of the system. Representative plots of KFM results for SAMs of **7**, **7**$^{+}$PF$_6^{-}$, and **7**-TCNE are shown in Figure 10 along with results from control experiments on SAMs of ferrocenylpentanethiol (**8**) and the ferrocenium PF$_6^{-}$ analogue **8**$^{+}$PF$_6^{-}$. Comparing ferrocene and ferrocenium PF$_6^{-}$ based SAMs demonstrates that the large increase in polarizability stems from the delocalized charge on the TTF^{+} and not simply from the charge-separated ionic character.

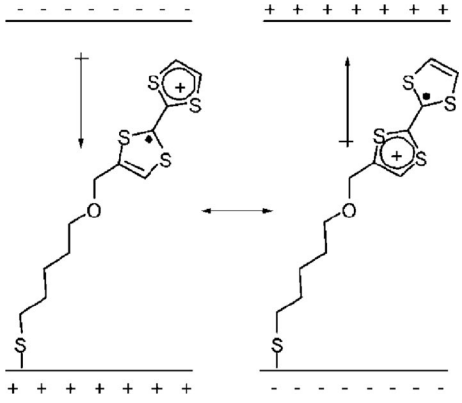

Scheme 4. Depiction of **7**$^{+}$ opposing an applied electric field.

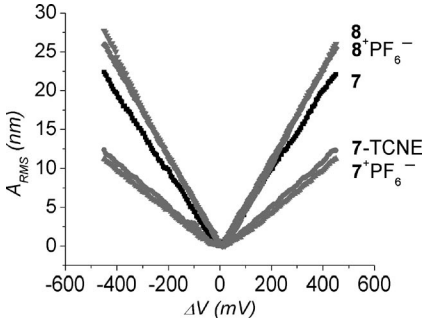

Figure 10. Representative KFM amplitude responses of **7**, **7**-TCNE, **7**$^{+}$PF$_6^{-}$, **8**, and **8**$^{+}$PF$_6^{-}$. Smaller slopes indicate greater electrostatic polarizabilities.

While the Robin-Day Class III delocalized TTF^{+} exhibited increased *polarizability*, Class II and II–III compounds are expected to exhibit *bistability*. To this end, self-assembled monolayers of Class II biferrocenyl derivatives are currently under investigation.

7. Summary and Outlook

In this microreview, we have mapped out key results from our group from the last ten years. This included studies which focused on physical understanding of mixed-valence systems that approach delocalization by estimating picosecond lifetimes from dynamically coalesced IR bandshapes and clarifying the role of solvent in the localized-to-delocalized transition, as well as applied studies investigating supramolecular cooperativity and electrostatic control of molecular electronic distribution. As with any field of research, each new discovery inspires new questions which will deepen our understanding of the systems we study. A few areas for future research that we think will be particularly fruitful are briefly detailed below.

Certainly our research has contributed to understanding the important role of solvent in Class II/III mixed-valence systems, but we are still far from a unifying theory for the localized-to-delocalized transition in mixed valency. As outlined succinctly in a recent review[35] the ultimate challenge lies in defining a theory whereby probing nearly delocalized systems by systematic experimentation provides physically meaningful quantities. In this light, the most obvious future contribution from our group will be a systematic analysis of the intervalence charge-transfer bands of the monoanionic ruthenium clusters which range from localized-to-delocalized in behaviour. We are poised to address important theoretical questions. Systematically modifying the ancillary ligands and the bridge to tune electronics, varying the solvent and temperature, and freezing the solvent will elucidate the relative effects of each change to the system, and allow new predictions for molecular events which occur on the picosecond timescale.

Ultrafast 2D infrared spectroscopy, a vibrational analogue of 2D NMR spectroscopy, is an exciting new technique which we plan to employ in our future work.[36] With femtosecond time resolution, 2D IR will enable independent estimates of rate constants for electron transfer, and will provide further insight into solvent-solute dynamics.

Class II bistable systems such as the biferrocenium monocation will allow a systematic study of molecular electronic switching mediated by an electric field when oriented in a monolayer and analyzed like the TTF-based monolayers described above. These will be investigated within the framework of symmetric and nearly symmetric mixed-valence systems, and many of the common methods for analy-

sis (IR, UV/Vis, Mössbauer) can be applied. This work will subsequently be extended to surface-based analogues of the ruthenium clusters, where ultrafast electron transfer can be investigated by IR methods. These studies will not only give early insight into mixed valency in ordered monolayers but demonstrate the utility of ultrafast mixed-valence systems in nanotechnology and work toward molecular computing.

Acknowledgments

We gratefully acknowledge support from the US National Science Foundation (NSF) (CHE-0616279).

[1] M. B. Robin, P. Day, *Adv. Inorg. Chem. Radiochem.* **1967**, *10*, 247.
[2] a) N. S. Hush, *Prog. Inorg. Chem.* **1967**, *8*, 391; b) C. Creutz, H. Taube, *J. Am. Chem. Soc.* **1969**, *91*, 3988–3989.
[3] T. Ito, T. Hamaguchi, H. Nagino, T. Yamaguchi, J. Washington, C. P. Kubiak, *Science (USA)* **1997**, *277*, 660–663.
[4] J. C. Salsman, S. Ronco, C. H. Londergan, C. P. Kubiak, *Inorg. Chem.* **2006**, *45*, 547–554.
[5] C. H. Londergan, J. C. Salsman, S. Ronco, L. M. Dolkas, C. P. Kubiak, *J. Am. Chem. Soc.* **2002**, *124*, 6236–6237.
[6] K. D. Demadis, C. M. Hartshorn, T. J. Meyer, *Chem. Rev.* **2001**, *101*, 2655–2685.
[7] S. D. Glover, B. J. Lear, C. Salsman, C. H. Londergan, C. P. Kubiak, *Philos. Trans. R. Soc. Ser. A* **2008**, *366*, 177–185.
[8] B. J. Lear, S. D. Glover, J. C. Salsman, C. H. Londergan, C. P. Kubiak, *J. Am. Chem. Soc.* **2007**, *129*, 12772–12779.
[9] N. J. Sutin, *Prog. Inorg. Chem.* **1983**, *30*, 441.
[10] P. F. Barbara, W. Jarzeba, *Acc. Chem. Res.* **1988**, *21*, 195–199.
[11] J. J. Turner, *Handbook of Vibrational Spectroscopy*, John Wiley & Sons Ltd., **2002**, p. 101–127.
[12] M. L. Horng, J. A. Gardecki, A. Papazyan, M. Maroncelli, *J. Phys. Chem.* **1995**, *99*, 17311–17337.
[13] C. H. Londergan, C. P. Kubiak, *J. Phys. Chem. A* **2003**, *107*, 9301–9311.
[14] P. Y. Chen, T. J. Meyer, *Inorg. Chem.* **1996**, *35*, 5520–5524.
[15] R. E. D. McClung, *Vibex GL*, *Program for the simulation of IR spectra of exchanging systems.*
[16] J. D. Badjic, A. Nelson, S. J. Cantrill, W. B. Turnbull, J. F. Stoddart, *Acc. Chem. Res.* **2005**, *38*, 723–732.
[17] B. J. Lear, C. P. Kubiak, *J. Phys. Chem. B* **2007**, *111*, 6766–6771.
[18] a) R. Baudry, O. Kalchenko, I. Dumazet-Bonnamour, F. Vocanson, R. Lamartine, *J. Chromatogr. Sci.* **2003**, *41*, 157–163; b) A. F. D. de Namor, R. M. Cleverley, M. L. Zapata-Ormachea, *Chem. Rev.* **1998**, *98*, 2495–2525; c) C. D. Gutsche, *Calixarenes*, The Royal Society of Chemistry, **1989**, p. 167–172.
[19] a) T. Ito, N. Imai, T. Yamaguchi, T. Hamaguchi, C. H. Londergan, C. R. Kubiak, *Angew. Chem. Int. Ed.* **2004**, *43*, 1376–1381; b) J. C. Salsman, C. P. Kubiak, *J. Am. Chem. Soc.* **2005**, *127*, 2382–2383.
[20] F. Barriere, N. Camire, W. E. Geiger, U. T. Mueller-Westerhoff, R. Sanders, *J. Am. Chem. Soc.* **2002**, *124*, 7262–7263.
[21] a) S. Baddam, B. E. Bowler, *J. Am. Chem. Soc.* **2005**, *127*, 9702–9703; b) G. McLendon, K. Pardue, P. Bak, *J. Am. Chem. Soc.* **1987**, *109*, 7540–7541; c) M. A. O'Neill, H. C. Becker, C. Z. Wan, J. K. Barton, A. H. Zewail, *Angew. Chem. Int. Ed.* **2003**, *42*, 5896–5900; d) J. S. Zhou, N. M. Kostic, *J. Am. Chem. Soc.* **1993**, *115*, 10796–10804.
[22] a) R. C. Rocha, H. E. Toma, *Inorg. Chem. Commun.* **2001**, *4*, 230–236; b) H. Tannai, K. Tsuge, Y. Sasaki, *Inorg. Chem.* **2005**, *44*, 5206–5208.
[23] E. Katz, R. Baron, I. Willner, *J. Am. Chem. Soc.* **2005**, *127*, 4060–4070.
[24] D. J. Campbell, B. R. Herr, J. C. Hulteen, R. P. VanDuyne, C. A. Mirkin, *J. Am. Chem. Soc.* **1996**, *118*, 10211–10219.
[25] D. G. Walter, D. J. Campbell, C. A. Mirkin, *J. Phys. Chem. B* **1999**, *103*, 402–405.
[26] B. J. Lear, C. P. Kubiak, *Inorg. Chem.* **2006**, *45*, 7041–7043.
[27] a) H. Qi, S. Sharma, Z. H. Li, G. L. Snider, A. O. Orlov, C. S. Lent, T. P. Fehlner, *J. Am. Chem. Soc.* **2003**, *125*, 15250–15259; b) Z. H. Li, A. M. Beatty, T. P. Fehlner, *Inorg. Chem.* **2003**, *42*, 5707–5714; c) Z. H. Li, T. P. Fehlner, *Inorg. Chem.* **2003**, *42*, 5715–5721.
[28] *Emerging Research Devices*, International Technology Roadmap for Semiconductors **2005**, 27–28.
[29] J. C. Goeltz, C. P. Kubiak, *J. Phys. Chem. C* **2008**, *112*, 8114–8116.
[30] a) D. O. Cowan, C. Levanda, J. Park, F. Kaufman, *Acc. Chem. Res.* **1973**, *6*, 1–7; b) K. Prassides (Eds.), *Mixed Valency Systems: Applications in Chemistry, Physics, and Biology*, Kluwer Academic Publishers, Dordrecht, The Netherlands, **1990**, p. 247–260.
[31] a) J. Garin, J. Orduna, S. Uriel, A. J. Moore, M. R. Bryce, S. Wegener, D. S. Yufit, J. A. K. Howard, *Synthesis* **1994**, 489–493; b) M. A. Herranz, L. Yu, N. Martin, L. Echegoyen, *J. Org. Chem.* **2003**, *68*, 8379–8385.
[32] J. C. Stires, E. J. McLaurin, C. P. Kubiak, *Chem. Commun.* **2005**, 3532–3534.
[33] a) O. Cherniavskaya, L. W. Chen, V. Weng, L. Yuditsky, L. E. Brus, *J. Phys. Chem. B* **2003**, *107*, 1525–1531; b) S. Howell, D. Kuila, B. Kasibhatla, C. P. Kubiak, D. Janes, R. Reifenberger, *Langmuir* **2002**, *18*, 5120–5125; c) T. Nakamura, E. Koyama, Y. Shimoi, S. Abe, T. Ishida, K. Tsukagoshi, W. Mizutani, H. Tokuhisa, M. Kanesato, I. Nakai, H. Kondoh, T. Ohta, *J. Phys. Chem. B* **2006**, *110*, 9195–9203; d) N. Saito, S. H. Lee, I. Takahiro, J. Hieda, H. Sugimura, O. Takai, *J. Phys. Chem. B* **2005**, *109*, 11602–11605.
[34] D. Sarid, *Scanning Force Microscopy*, revised, Oxford University Press, New York, **1994**.
[35] D. M. D'Alessandro, F. R. Keene, *Chem. Soc. Rev.* **2006**, *35*, 424–440.
[36] a) J. F. Cahoon, K. R. Sawyer, J. P. Schlegel, C. B. Harris, *Science (USA)* **2008**, *319*, 1820–1823; b) N. H. Ge, M. T. Zanni, R. M. Hochstrasser, *J. Phys. Chem. A* **2002**, *106*, 962–972; c) K. Kwak, J. R. Zheng, H. Cang, M. D. Fayer, *J. Phys. Chem. B* **2006**, *110*, 19998–20013.

Received: September 11, 2008
Published Online: December 12, 2008

